Shear Studs Effect on the Seismic Behavior of Steel Beam–Concrete-Filled Tube Column Connections

Mohsen Alikhani[1], Shahin Borzoo[2,*] and Saeed Najafi[3]

[1]Department of Civil Engineering, K. N. Toosi University of Technology, Tehran, Iran

[2]Civil Engineering Department, Technical University of Buein Zahra, Buein Zahra, Qazvin, 3451745346, Iran

[3]Department of Earthquake Engineering, Tarbiat Modares University, Tehran, Iran

Abstract: The purpose of this study is to investigate the effect of the geometrical shape of the shear studs of steel-concrete composite column on the structural behavior of the steel beam to column connection. The effect of the desired parameter on the force-displacement curve, strain energy, internal energy, and the amount of plastic dissipated energy is investigated. In this research, 19 models were developed in ABAQUS finite element software using L-shaped, U-shaped and T-shaped shear studs. The results show that by increasing the parameters such as the stiffness and shear resistance of the steel-concrete composite column system, their bearing capacity increases. Finally, force-displacement interaction diagrams have been developed for steel-concrete composite columns. The results showed that the use of a U-shaped shear stud can increase the column tolerated forces by 295%. Also, the most increases are related to models with U-shaped studs, and then models with L-shaped studs, in which the forces have increased by 233%. The most increase in displacement belongs to U-shaped studs, which showed a 52% increase in displacement capacity of the connection.

Keywords: Shear stud, Composite column filled with concrete, Finite element, Connection, Force-displacement curve.

1. INTRODUCTION

Composite, concrete-filled tube (CFT) is increasingly used as a column or column-beam in braced structures and moment frames. Tube columns filled with concrete made from welded plates and tubes, which are used in the world's tallest buildings (Lin *et al*., 2023). Also, in Japan, this method is commonly used for bridge columns (Huang *et al*., 2023; Zhou *et al*., 2023). Concrete-filled members have better efficiency than steel sections, reinforced concrete, or steel reinforced with concrete. The seismic design of CFTs in the moment-resistant frames significantly increases the resistance to weight ratio, and due to the confinement of concrete and continuous bracing, tube columns cause a delay in local buckling (Borzoo *et al*., 2016). The modified dissipation behavior is evident in comparison with normal steel frames. Also, the increase in ductility and stiffness effectively acts in moment resistance, tension, and axial pressure.

Ding *et al*., (2016) investigated the mechanical behavior of concrete-filled steel tubular columns that were placed inside the steel chamber and subjected to axial load. They developed a theoretical formula to predict the load capacity of CFT columns that were subjected to axial load based on the experimental and numerical model. Analyses of L-shaped CFT column frames with buckling-restrained and unrestrained steel plate shear walls reveal the importance of connection details on cyclic performance and energy dissipation (Amer *et al*., 2023). On the other hand, axial load behavior is critical in CFT columns, especially when considering complex geometries such as rectangular wave-shaped ribs (Song *et al*., 2024) or multi-cell configurations (Pahlavannejad Tabarestani *et al*., 2025). These configurations influence load distribution and buckling resistance. Numerical analyses show complex behaviors such as punching shear at shear head connections between CFT columns and flat reinforced concrete slabs (Nguyen-The *et al*., 2024). Moreover, experimental and numerical investigations on moment connections, such as I-beam to CFT column with pipe-stiffened diaphragms (Habibi *et al*., 2023) and tube-in-tube rigid beam connections, reveal critical insights for ensuring rotational capacity and connection rigidity in moment-resisting frames (Razavi *et al*., 2023).

The reviewed literature clearly demonstrates the multifaceted nature of CFT column behavior, where geometry, material properties, reinforcement detailing, connection design, and loading conditions interplay to define performance. While significant progress has been made in experimental and numerical characterization, one of the main uncertainties is the connection design between outer steel tubes with filled concrete, especially with complex diaphragm stiffening,

*Address correspondence to this author at Civil Engineering Department, Technical University of Buein Zahra, Buein Zahra, Qazvin, 3451745346, Iran; E-mail: Sh.borzoo@bzte.ac.ir

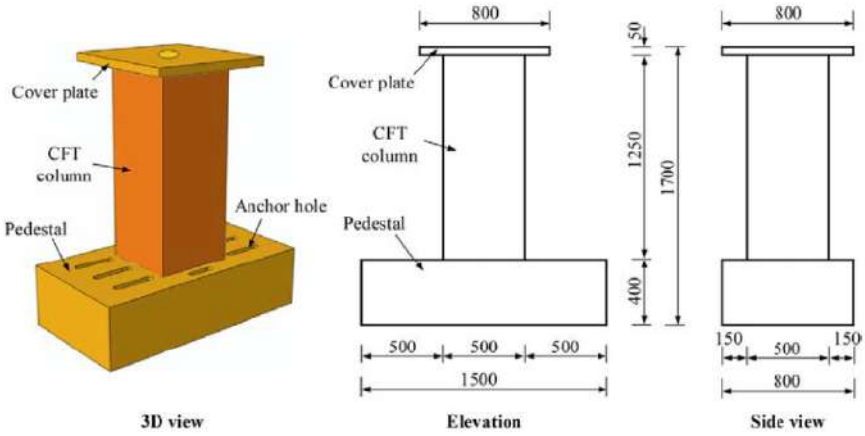

Figure 1: Geometry and dimensions of the validation model (Wang *et al*., 2019).

which warrants further research to develop standardized design guidelines. Habibi *et al*., (2023) present an experimental and numerical investigation of two full-scale I-beam to concrete-filled tube (CFT) column internal-diaphragm moment connection specimens. Li *et al*., (2023) offered an innovative form of manufactured H-shaped steel beam to concrete-filled steel tubular (CFST) column connections. The performance of this beam to column connection was examined through cyclic loading. The thickness and the yield stress of the column steel, and the distance between the transfer sleeve and the beam flange were the main parameters. The hysteretic performance, bending stiffness, resistance, and energy consumption of the connection were investigated. The innovative connection exhibited appropriate bending and energy dissipation capacity. The thickness and yield stress of the tube notably improved the bending capacity of the column-column connection and the shear displacement. Guo *et al*., (2023) evaluated the interactional behavior of the core concrete and steel tube in large rectangular concrete-filled steel tubular (LSCFT) columns under applied direct vertical load. LSCFT column specimens with different specifics were tested under axial compression to investigate the mechanical behavior and load transferring mechanism of the LSCFT columns with a distributive beam. The experimental results showed that the bearing capacity of the LSCFT columns without a distributive beam is close to the yield capacity of the steel tube.

This paper aims to develop some finite element analyses to evaluate the form, dimension, and spacing of shear studs on the interaction of concrete and steel columns, by investigating the force-displacement curve, strain energy, internal energy, and the amount of plastic dissipated energy. First, a validation model is developed to set analytical parameters in a real condition. In the next a parametric study is done to evaluate the study variables. For this purpose, 18 numerical models and a base model without any shear stud are developed and discussed.

2. ANALYTICAL MODELING

2.1. Validation Model

The study used for verification is an experimental test by Wang *et al*., (2019). This research investigated the behavior of CFST columns made with different shear studs. Their study was conducted in an experimental procedure, and 12 samples of CFST columns with different numbers of shear studs were examined. Also, the resistance of concrete, load capacity, and axial displacement capacity were investigated.

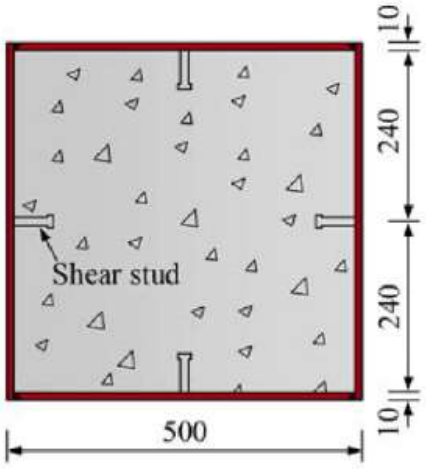

Figure 2: Section of the validation model (Wang *et al*., 2019).

The validated model is a steel column with the same thickness of 10 mm on each side, which is made of 4 steel plates that are welded together. More

addition, the studs are welded to the steel plates on the inner side. The studs have a radius of 13 mm and their length is 55 mm, and their spacing in the vertical direction is 160 mm.

2.1.1. Material Properties

To model the steel material, the elastic-plastic properties are considered (Table **1**). For concrete material, the average compressive strength of the cubic sample is 43.8 MPa. A steel plate with dimensions of 800 x 800 mm and a thickness of 50 mm is placed on the top of the sample (Wang *et al*., 2019).

The elastic property is used to define the concrete material, and the plastic damage property is used to develop the cracks in the concrete material according to Table **2**. The other related properties of concrete damage are presented in Table **3**.

2.1.2. Interactions and Loading

To define the interaction between the steel column and the concrete, the tie constraints are selected (Najafi & Borzoo, 2022). To model the contact mode between these materials, the tangent behavior mode and the friction behavior are developed (Najafi *et al*., 2022). To consider the normal behavior, “hard” contact is selected for pressure-overclosure (Najafi *et al*., 2025). The loading protocol is adopted based on Wang *et al*., (2019). In the early loading phase, the displacement amplitude was 5 mm, 10 mm, 15 mm, and 20 mm for one cycle, and then the displacement amplitude was three cycles from the amplitude of 25 mm. The cyclic lateral loading was terminated when the load-carrying capacity of the column dropped to 85% of the maximum strength or severe tearing damage of the steel tube was observed. After developing the numerical model, a comparison has been made between the numerical results and the experimental results by (Wang *et al*., 2019). As can be seen from the force-displacement diagram and the final damage forms, the validation of the numerical model is at a good level (Figure **6**).

Table 1: Specification of Steel Material (Wang *et al*., 2019)

Poisson ratio	Modulus of elasticity (Mpa)	Plastic properties	
		Yield Stress (Mpa)	Plastic Strain
0.3	201000	300.4	0
		443.3	0.1

Table 2: Specifications of Concrete Materials (Wang *et al*., 2019)

Mass Density (kg/m^3)	Young’s Modulus (MPa)	Poisson’s Ratio	Yield Stress (Mpa)	Inelastic Strain	Yield Stress (Mpa)	Cracking Strain
			compression		tension	
2500	33835	0.2	320	0	62	0
			329.03	0.00128	33.33	0.001017987
			438	0.002231921	19.30	0.001809425
			394.76	0.002731921	13.07	0.002577852
			286.84	0.003231921	9.69	0.003337839
			178.21	0.003731921	7.61	0.00409399
			103.86	0.004231921	6.22	0.004848114
			60.39	0.004731921	4.95	0.005851848
					3.75	0.0073554
					2.72	0.009558436

Table 3: The Crack Coefficients of Concrete Materials

Dilation L-shape	Eccentricity	fb0/fc0	k	Viscosity Parameter
38	0.1	1.16	0.667	0.01

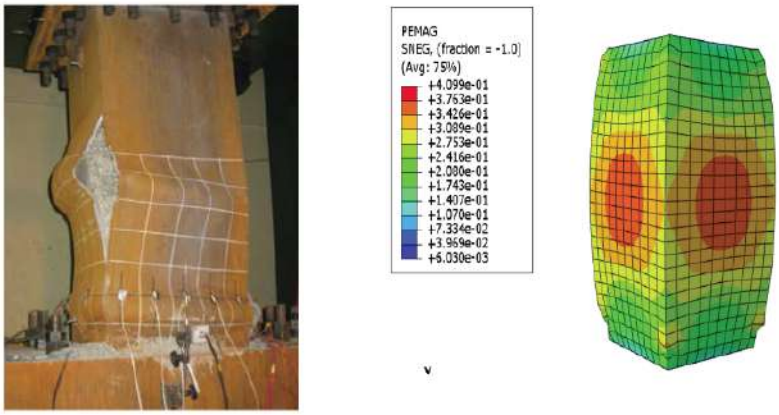

Figure 3: Comparing the maximum plastic strains in the numerical model with experimental model.

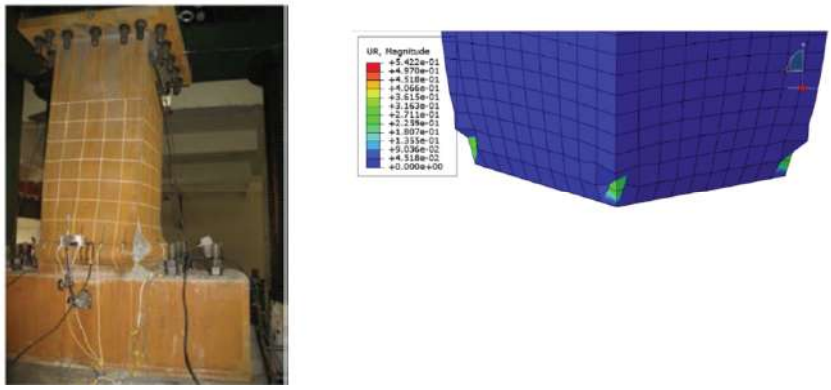

Figure 4: Comparing the maximum strains and moments in the numerical model with experimental model.

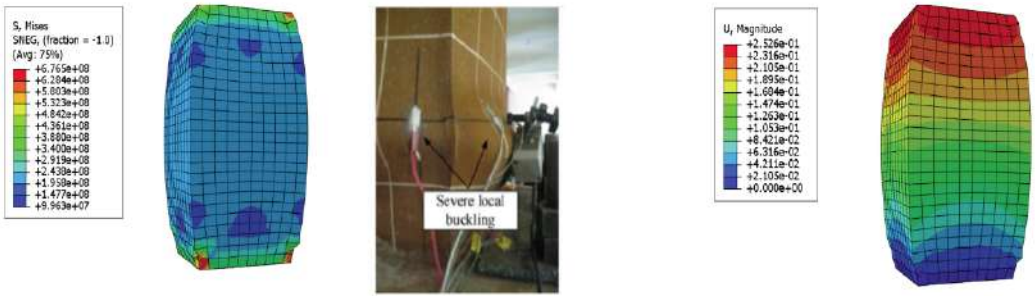

Figure 5: Comparing the maximum stress and displacement in the numerical model with experimental model.

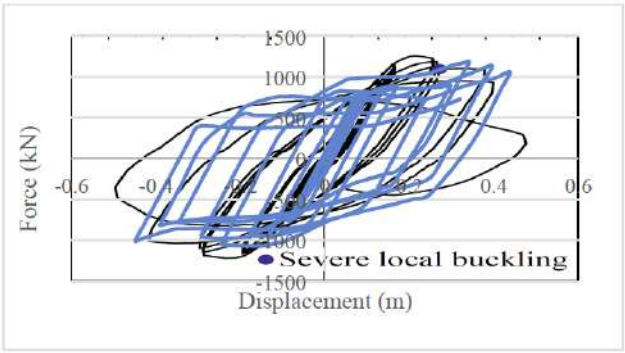

Figure 6: Comparison of the force-displacement diagram of the experimental SC-1-0.4 model with the validation numerical model.

3. ANALYTICAL PARAMETRIC STUDY

In this research, 18 numerical models of composite CFT columns with outer steel section and filled concrete are built, which have different kinds of shear studs. The models have been analyzed for three types of shear studs as L, U, and T forms. The boundary conditions are set according to the verification numerical model at the top and bottom of the column. In all models, a cyclic force is applied to the tip of the connected beam to column, and the rotation measurement criterion is considered in the part of the connection between the beam and the column. In this

Table 4: Characteristics of Models

Stud height	Type of stud	Studs spacing	Studs thickness	Length of column	Model Name
4	L-shape	18 cm	10 mm	150 cm	L- At 18- 4
6	L-shape	18 cm	10 mm	150 cm	L- At 18- 6
8	L-shape	18 cm	10 mm	150 cm	L- At 18- 8
4	L-shape	36 cm	10 mm	150 cm	L- At 36- 4
6	L-shape	36 cm	10 mm	150 cm	L- At 36- 6
8	L-shape	36 cm	10 mm	150 cm	L- At 36- 8
4	U-shaped	18 cm	10 mm	150 cm	U- At 18- 4
6	U-shaped	18 cm	10 mm	150 cm	U- At 18- 6
8	U-shaped	18 cm	10 mm	150 cm	U- At 18- 8
4	U-shaped	36 cm	10 mm	150 cm	U- At 36- 4
6	U-shaped	36 cm	10 mm	150 cm	U- At 36- 6
8	U-shaped	36 cm	10 mm	150 cm	U- At 36- 8
4	T-shaped	18 cm	10 mm	150 cm	At 18- 4 T-
6	T-shaped	18 cm	10 mm	150 cm	At 18- 6 T-
8	T-shaped	18 cm	10 mm	150 cm	At 18- 8 T-
4	T-shaped	36 cm	10 mm	150 cm	At 36- 4 T-
6	T-shaped	36 cm	10 mm	150 cm	At 36- 6 T-
8	T-shaped	36 cm	10 mm	150 cm	T- At 36- 8

research, the four selected variables are the number of studs, their geometric shape, their length, and the distance of the studs along the height of the column. In all models, the cross section of the concrete and steel wall is considered the same. Table **4** shows all the developed numerical models in this research with the details of their construction geometry. As can be seen in Table **4**, there are three modes based on the length of the studs. The studs are selected in three lengths of 4, 6, and 8 cm. The studs have three L, U, and T-shaped.

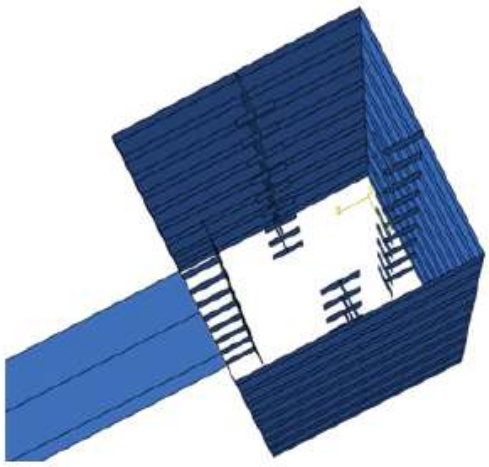

Figure 7: Internal view of shear studs.

The distribution of stresses and deformations in each model is obtained. Figures **8** and **9** show the strains in the model with T-shaped studs. As can be seen, this type of stud is completely embedded in concrete due to its special geometry, and therefore the plastic strains have reached the value of nearly $1.3e^{-3}$ and has largely prevented the deformation of the column.

Figure **10** shows the strains in the steel wall of models with L-shaped studs, as can be seen in this figure, due to the less involvement of this type of stud in concrete, the ultimate strain limit of this model is less and also the displacements in the connection of the beam flange to the column has been increased, which is not desirable.

Figure **11** shows the strains in the model with U-shaped studs. This model has a higher strain bearing capacity than other models because it engages the steel column with the concrete by two wings. So that it can be seen that the strains have increased to a much higher extent, up to about $1.8e^{-2}$. Figure **12** shows the stresses in the model with T-shaped stud.

Figure **13** shows the stresses in the model with U-shaped studs. In this model, due to the engagement of

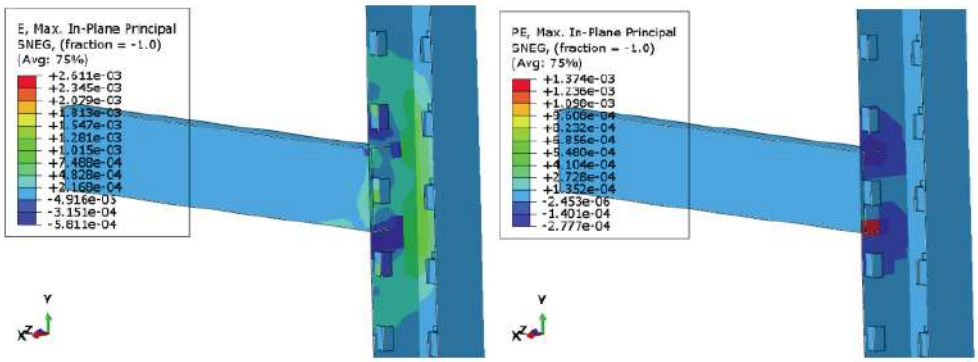

Figure 8: Display of elastic strains in models with T-shaped studs.

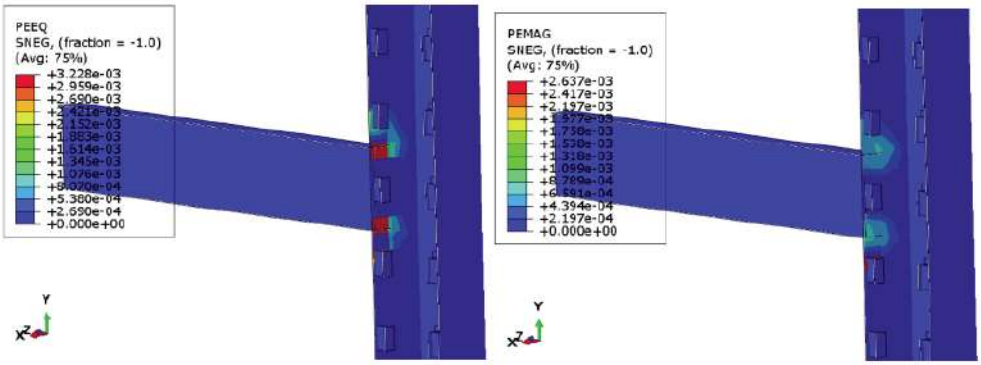

Figure 9: Display of plastic strains in models with T-shaped studs.

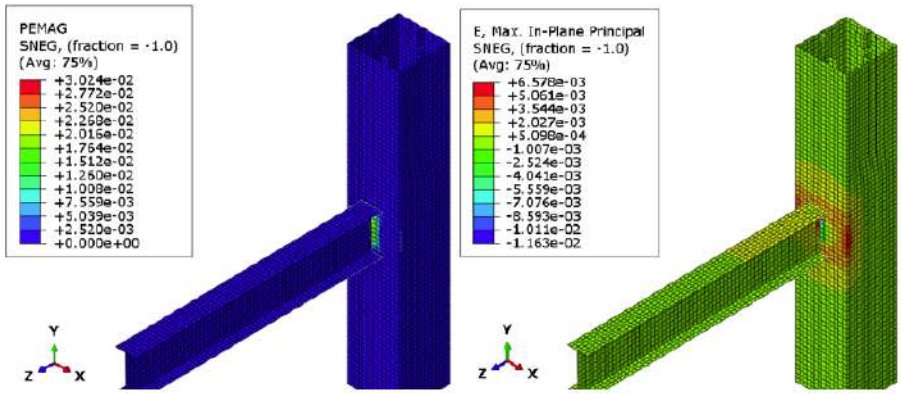

Figure 10: The strains in the models with L-shaped studs.

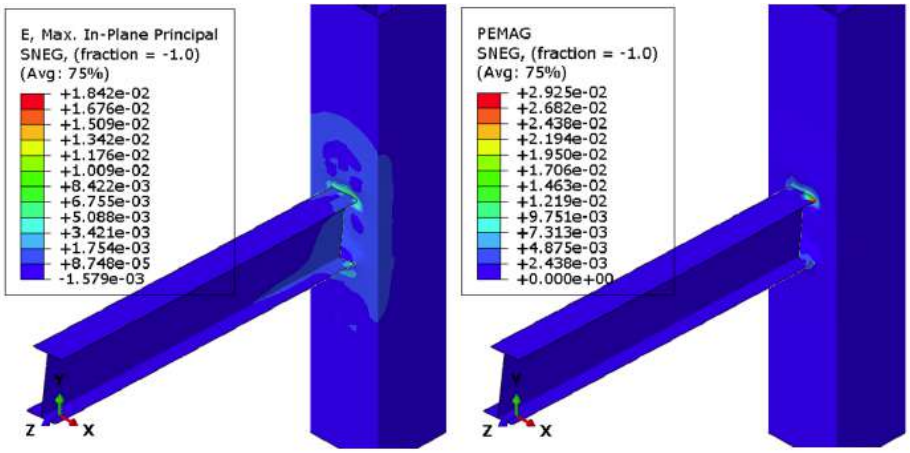

Figure 11: The strains in the models with U-shaped studs.

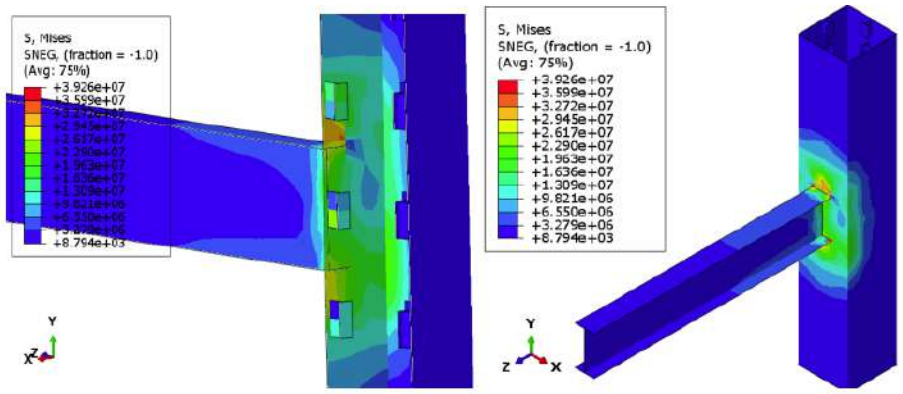

Figure 12: The stresses in the model with T-shaped studs.

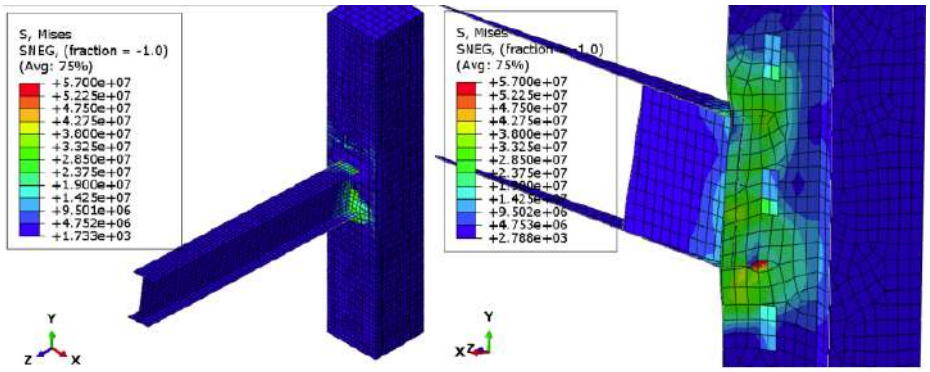

Figure 13: The stresses in the model with U-shaped studs.

the two wings of this stud in the concrete, it creates a proper connection between the concrete and the steel wall, and the distribution of stresses in the column and connection has usefully expanded in the connection point of the beam to the column and prevented the concentration of stress in one point, which is very favorable. So that there is no significant increase in the amount of stress at the connection of the beam to the column.

As can be seen in Figure **14**, the connection of the L-shaped stud is less than other two models, and the reason is the lower contact surface of this type of stud with concrete. This fact has caused the concentration of stresses at the connection of the beam flanges to the column. The stresses in the column plate should be increased, which is not desirable, and with increasing load, it will cause connection failure in this place.

Figures **15** to **17** show the graphical outputs from the analysis of the numerical models, including stress distribution in each case, strain distribution, displacement, and the points where yielding occurred. Considering that for concrete materials, the plastic

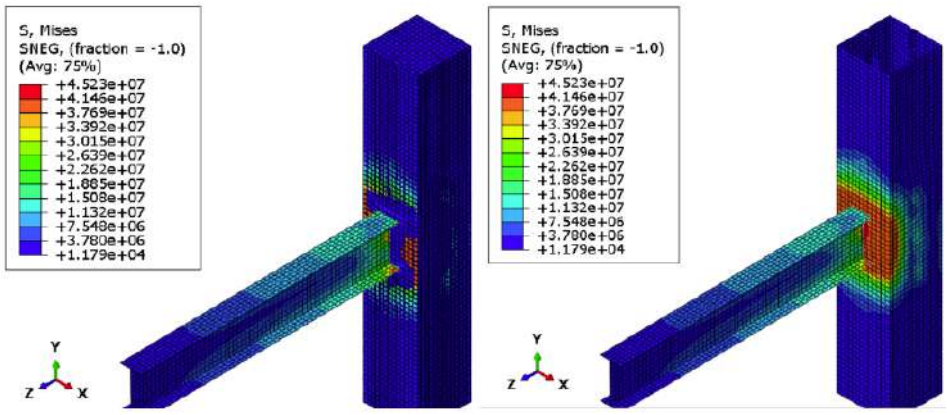

Figure 14: The stresses in the model with L-shaped studs.

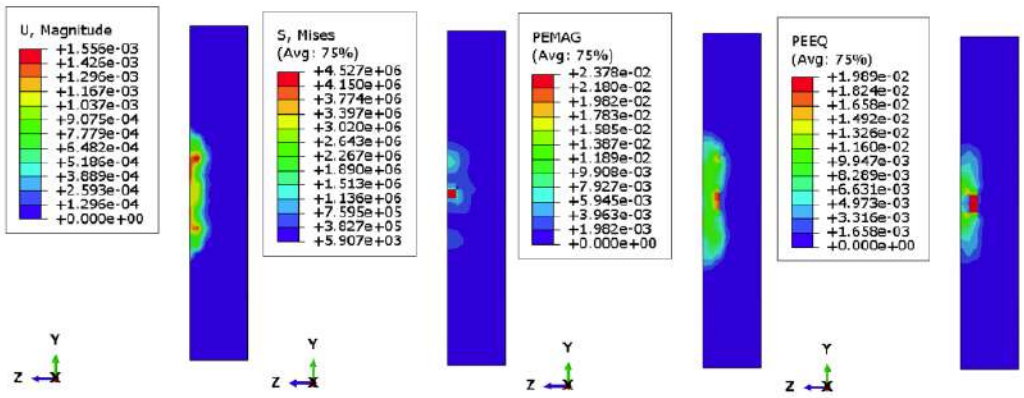

Figure 15: The graphic outputs of concrete in the model with a T-shaped stud.

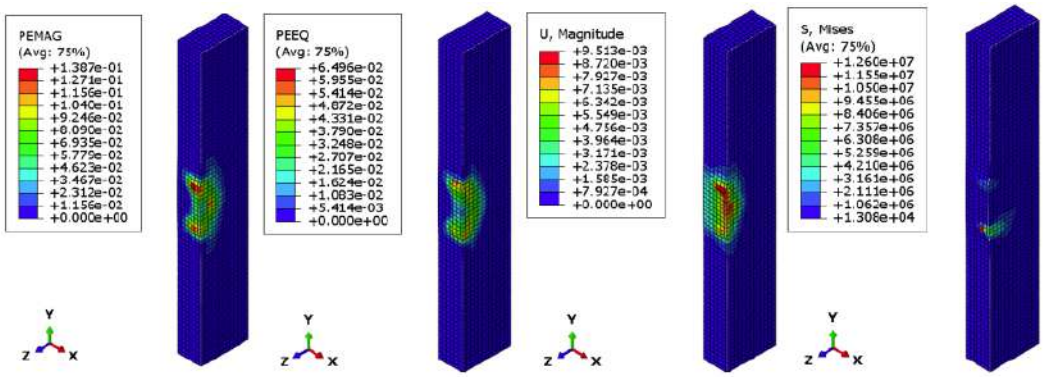

Figure 16: The graphic outputs of concrete in the model with a U-shaped stud.

compressive stress is 250 MPa and the final compressive stress is 300 MPa, if the compressive stress exceeds any of these values, plasticization or destruction of the composite column concrete will occur. Also, the final strain of concrete materials is considered to be 0.01. So, if the strain of concrete materials exceeds 0.01, it would lead to cracking failure and failure of composite columns in that area.

As can be seen in Figure **15**, the concrete trapped behind the stud blades has suffered a lot of strain up to about 2 mm. In addition, we will face concrete cracking in this area, and the stresses have also increased greatly in this part of the concrete. Regarding the change in displacement, it can be seen that due to the reciprocating loading of the beam at the connection point between the beam and the column web, and especially at the contact point between the column wings and the web, it has increased.

Since in the stud cutter, the concrete and steel walls are connected by two stud wings and the contact surface is larger, it can be seen that the stress concentration and also the point increase of the strain

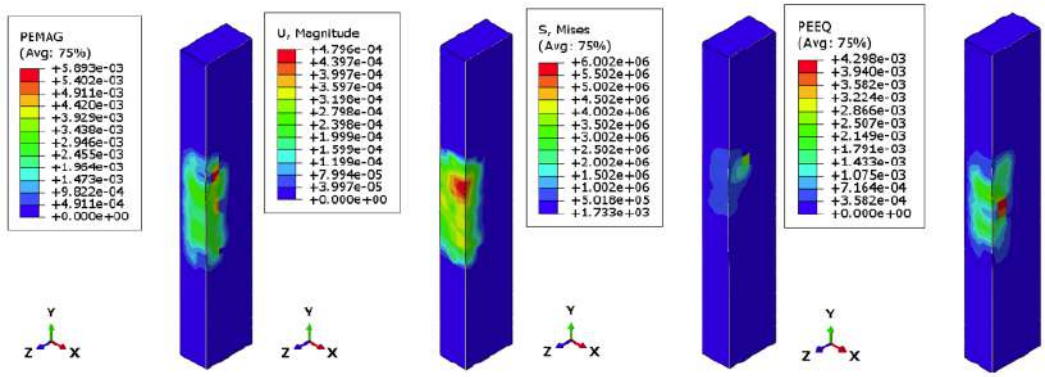

Figure 17: The graphic outputs of concrete in the model with a L-shaped studs.

have been greatly reduced. As in the previous model, the changes in the places where the wings of the beam join the column have been increased. The difference between this model and the model with a stud cutter is that the displacements at the junction of the beam and the column have also increased.

Figure **17** shows the fact that the reduction of the contact surface between the concrete and the shear studs has caused an increase in stress, strain, and displacements in the concrete of the composite column. So that it can be seen that the displacements are no longer limited to the beam-to-column connection and are created in a wide area of concrete. In addition to the fact that the stresses and strains have increased at the places where the studs are connected to the concrete, the stresses and strains have greatly increased in other surfaces of the connection area.

3.1. Force-Displacement Curve

From numerical models, the force-displacement curves have been drawn to compare the capacity and resistance of various types of steel-concrete composite columns. Figures **18** to **23** show the force-displacement curves in models with L-shaped studs. As can be seen in the models with studs made of L-shape, where the L-shaped wings are 4 cm, the force-displacement curves have many irregularities and do not have steady cycles. With the increase in the length of the wings of the L-shaped studs, the cycles have become more regular, and the force-displacement values have also increased. Finite element modeling was done in three parts. For this purpose, composite columns with different studs are analyzed.

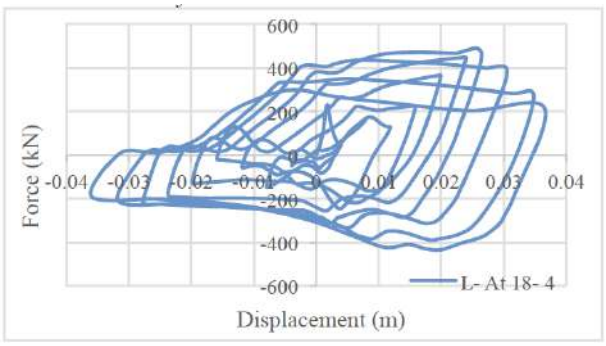

Figure 18: The force-displacement curve of the L-At 18-4 model.

In the models that the distance between their studs is less than 18 cm verse to the models that have 36 cm space between each stud, the maximum values of the tolerable force in models with 18 cm distance are higher, which are about twice as much as the models with 36 cm space.

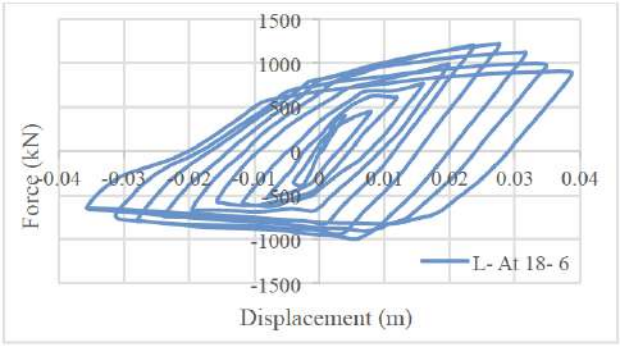

Figure 19: The force-displacement curve of the L-At 18-6 model.

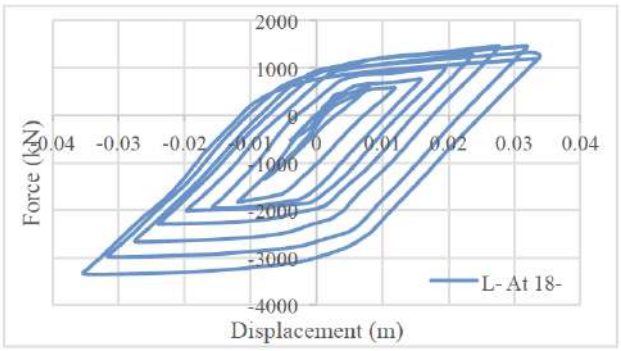

Figure 20: The force-displacement curve of the L-At 18-8 model.

The model with studs made by 4 cm L-shaped with a distance of 36 cm had almost the same load as the model of the same studs in size and shape, with a distance of 18 cm in the longitudinal axis of the column. But in the return cycles, the values of the force's endurance are greatly reduced.

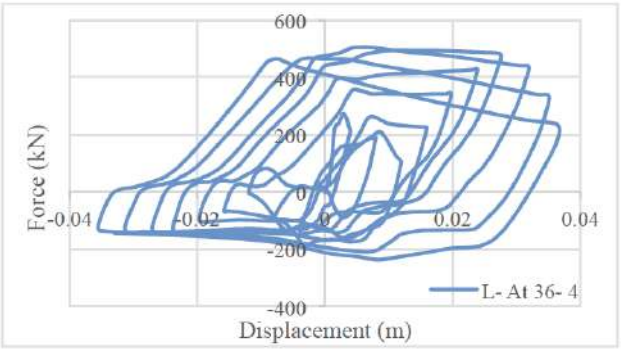

Figure 21: The force-displacement curve of the L-At 36-4 model.

Figure **23** shows the fact that when the length of the studs is added (8 cm in this model) and the distance between the studs in the longitudinal axis of the column increases, although the tolerable force values increase

in the tensile area of the diagram. But when the direction of the applied load is changing, in the pressure cycles of the loading, the tolerable force values have been greatly reduced, so that for the L-At18-8 model, this value has increased to 3600 kN, but for the L-At36-8 model, the compressive force value, at around 2500 kN, has been stopped.

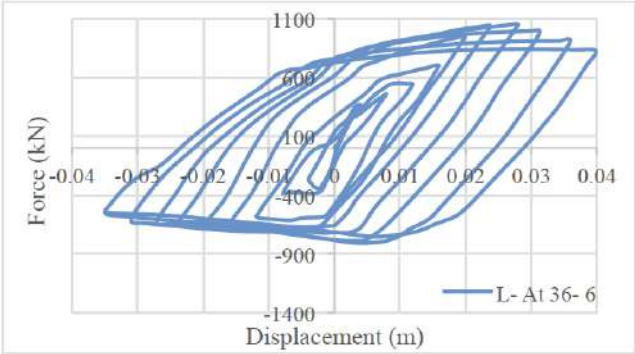

Figure 22: The force-displacement curve of the L-At 36-6 model.

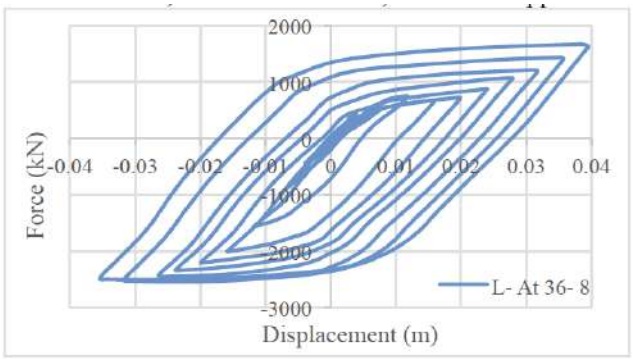

Figure 23: The force-displacement curve of the L-At 36-8 model.

Figures **24** to **29** show the curves related to the displacement force diagram of models with T-shaped studs. The first point about these curves is that the amount of force that can be tolerated by them is more than the models with studs made an L-shaped section. Also, unlike L-shaped studs that performed poorly in tensile cycles, these models are very strong in tensile cycles, and the reason for this is the proper connection of concrete and studs due to the geometry of T-shaped studs. Another point is that in models with T-shaped studs, except the T-At18-4 and T-At36-4 models, where the length of the studs is 4 cm, the rest of the models have regular cycles.

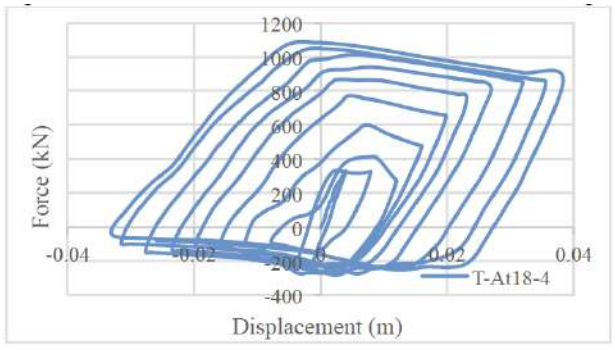

Figure 24: The force-displacement curve of the T-At 18-4 model.

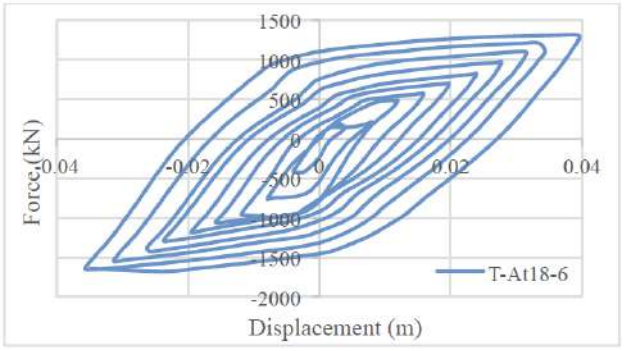

Figure 25: The force-displacement curve of the T-At 18-6 model.

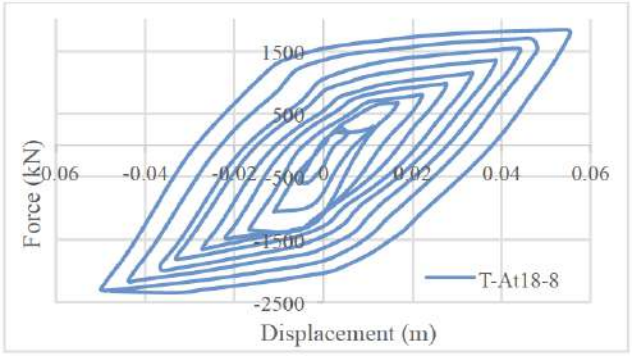

Figure 26: The force-displacement curve of the T-At 18-8 model.

Figure **27** shows relatively better performance of the T-at 18-4 compared to the T-at36-4 model, but the differences are not so significant.

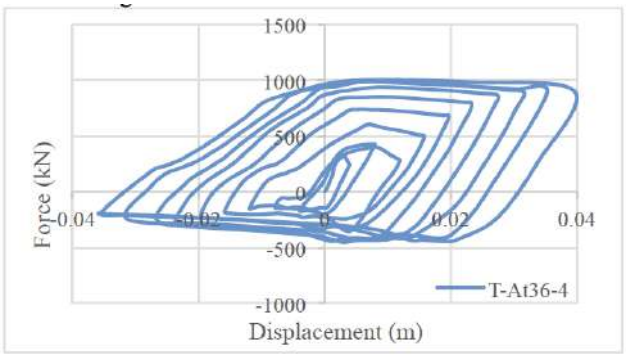

Figure 27: The force-displacement curve of the T-At 36-4 model.

Figures **28** and **29** show the force-displacement curves of T-At 36-6 and T-At 36-8 models, which show

regular cycles of these two models. Also, the force-displacement values for these two models are very favorable, so that the area inside the cycles of these curves has been usefully increased, and because the enclosed area inside the cycle has a direct relationship with ductility, these models have improved performance.

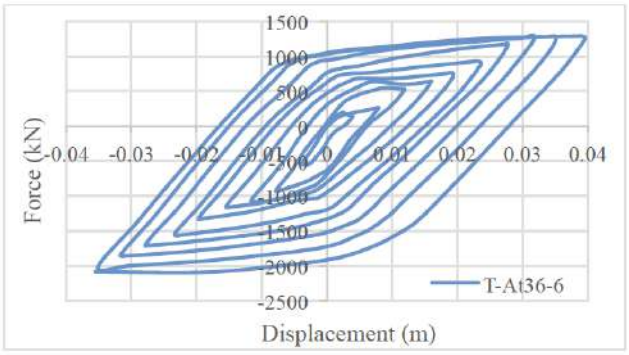

Figure 28: The force-displacement curve of the T-At 36-6 model.

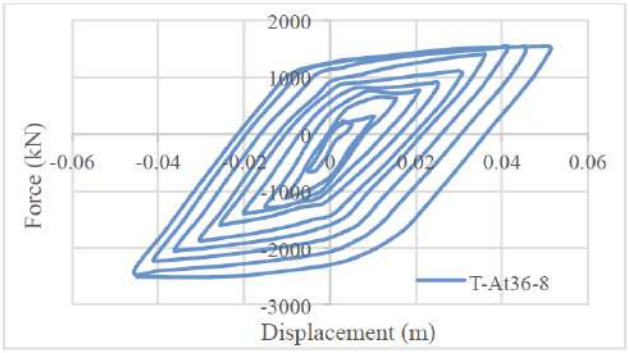

Figure 29: The force-displacement curve of the T-At 36-8 model.

Figures **30** to **35** show the curves related to the displacement force diagram of models with U-shaped studs. The first point about these curves is that the amount of force that can be tolerated by them is less than the models with T-shaped studs and more than the models with the L-shaped studs. Also, unlike other models, in tensile and compressive cycles, they have shown almost the same performance in terms of ultimate force, and the reason for this is the greater continuity of the studs compared to the models with studs made of L-shape, because the contact surface of the studs with the concrete is increased. Another point is that in these models, except the U-at18-8 and U-at36-8 models, where the length of the studs is 8 cm, the rest of the models have irregular cycles. The irregularity of the graphs may be due to the existence of two separate contact surfaces in each row of studs, which caused one of the stud wings to act in each cycle.

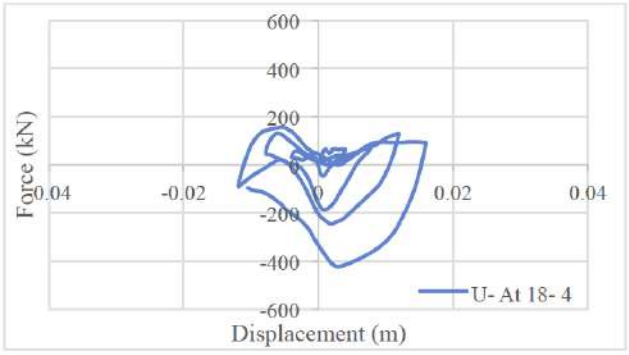

Figure 30: The force-displacement curve of the U-At 18-4 model.

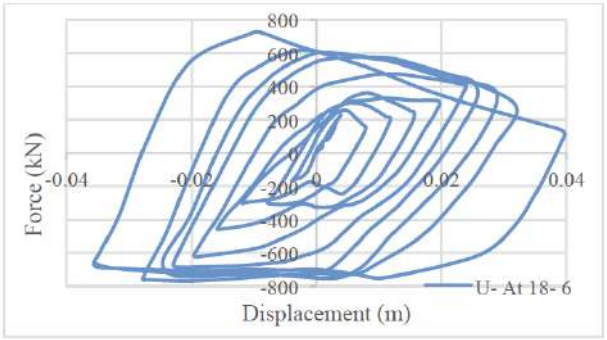

Figure 31: The force-displacement curve of the U-At 18-6 model.

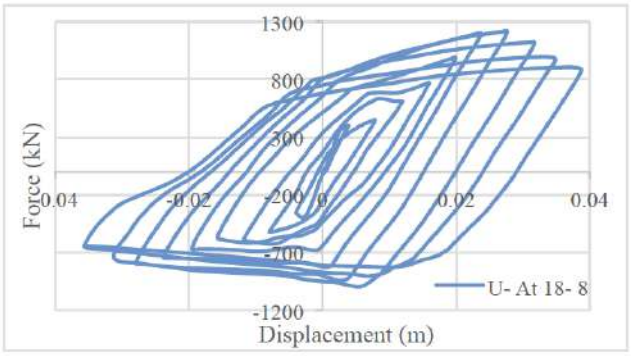

Figure 32: The force-displacement curve of the U-At 18-8 model.

Figures **33** to **35** show the curves related to the displacement force diagram of the models with U-shaped studs having 36 cm intervals along the column. The first point about these curves is that the irregularity of the force-displacement curves is much more noticeable in these models, and the U-at36-4 and U-at36-6 models have many irregularities in the cycles. Also, the U-at36-8 model got regular cycles and has performed much better in tension. The U-at36-8 model is weak in compression, while in the models that had U-shaped studs with 18 cm intervals, the curves were more regular and the performances in tension and compression were almost the same. The reason for this fact is the greater continuity of the studs compared

to the models with 36 cm intervals set, because the contact surface of the studs along the axis of the column with concrete is doubled. Another point is that in these models, except the U-At18-8 models, where the length of the studs is 8 cm, the rest of the models have irregular cycles.

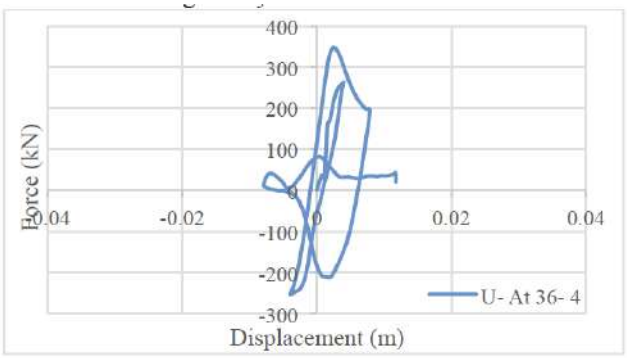

Figure 33: The force-displacement curve of the U-At 36-4 model.

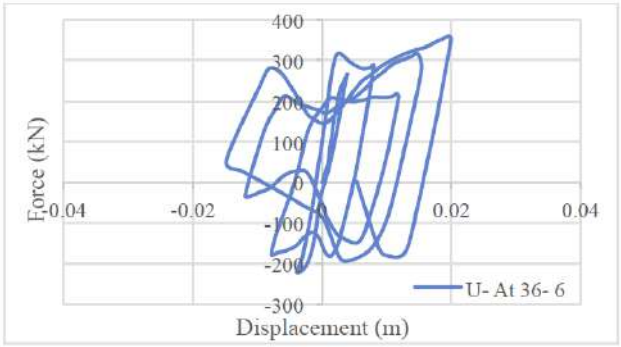

Figure 34: The force-displacement curve of the U-At 36-6 model.

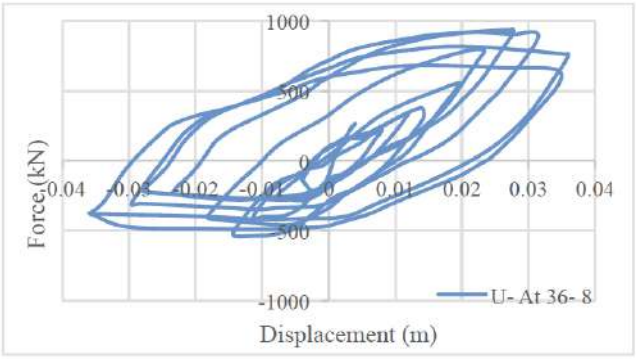

Figure 35: The force-displacement curve of the U-At 36-8 model.

In Figure **36**, to make a comparison between the system of composite columns with shear studs and without shear studs, the results of another model without studs are presented, as can be seen in this figure, despite the use of longitudinal and transverse reinforcements in the column as well as the steel wall, the resistance of the column against the load has not increased much. In this model, the maximum resistance of the column was even increased up to 4000 kN, which shows the effectiveness of this system. Of course, it is important to mention that this column has good plasticity in order to tolerate suitable displacements.

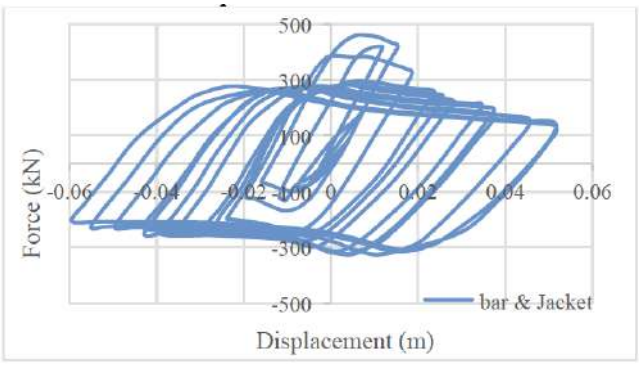

Figure 36: The force-displacement curve of the model without shear stud.

3.2. Comparison of Energy Values

Figures **37**, **38**, and **39** compare the values of internal energy, dissipated plastic energy, and strain energy in models with 18 cm distance stud spacing, respectively. As seen in Figure **37**, the internal energy of T-At18-8 and T-At18-6 models is higher than all models. After that, U-At18-8 and T-At18-4 models have the highest internal energy values. Also, models with corner cutters have the lowest amount of internal energy compared to other models, and models that have cutters of any shape and with a size of 4 cm also have a small amount of energy. But in Figures **38** and **39**, the results regarding the strain energy and the plastic energy dissipated are different; although the energy value of the models with stud cutters is higher, it is in a range close to other models. In these graphs, the highest energies are related to T-at18-8 and U-at18-8 models, but the difference with other models is not significant. This shows that this system will generally have a good energy dissipation against round-trip loads.

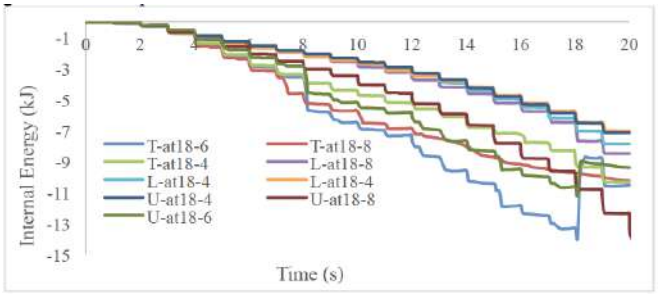

Figure 37: Comparison of the internal energy.

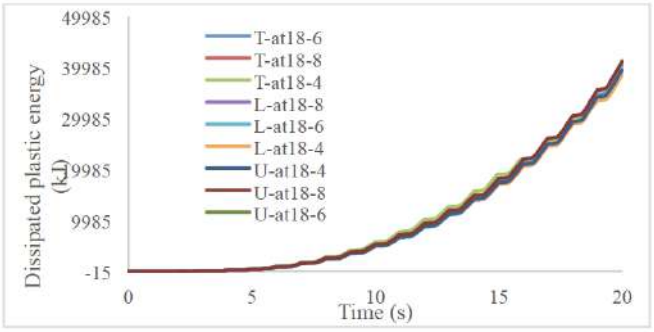

Figure 38: Comparison of the discarded plastic energy.

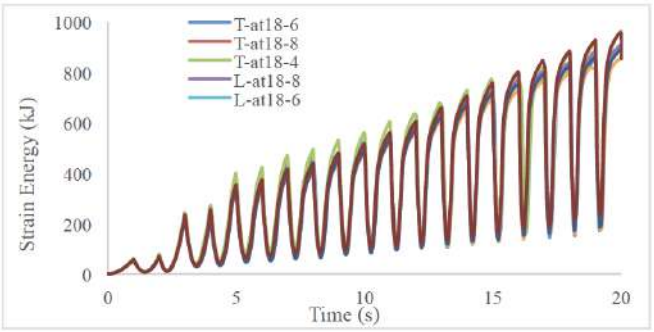

Figure 39: Comparison of the strain energy.

3.3. Maximum Force and Displacement

In this section, the numerical results of different models have been quantitatively compared with each other. As can be seen in Figure **40**, the maximum tolerable displacement among the models is related to the U-at18-8 model. After that, the U-at36-8 model has the highest amount of tolerable displacement before breaking. So, as can be seen, if resilience against high displacements is considered, it is desirable to use U-shaped studs. Also, it can be seen in Figure **40** that the other models are all in a certain range and their tolerable displacement is about 4 cm, so there is not much difference in terms of displacement using studs made of L-shaped or T sections.

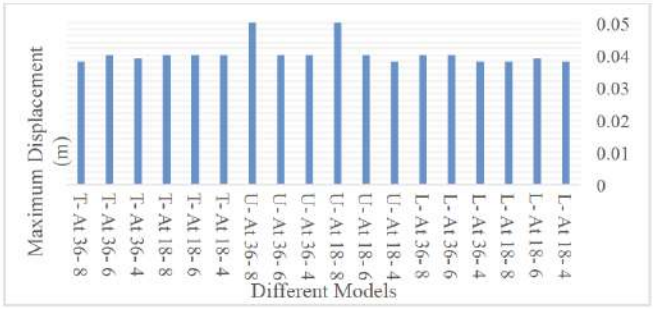

Figure 40: Comparison of the most tolerable displacement in different models.

Figure **41**, which is related to the comparison of forces, gives significant results. There is a lot of dispersion in the maximum tolerable force between different kinds of studs. The maximum tolerable force is again related to the U-at18-8 model. As seen, this model has both a good displacement and force tolerance, so the use of studs made of U sections will be beneficial. Since the tolerable force of the T-At36-4 model has a significant difference, shows that the use of U-shaped stud will not work if it does not have the proper length, and the distance between the studs be too large. This point also applies to the studs made of L-shapes, as it can be seen that the models L-At18-4 and L-At36-4 have the lowest value of tolerable forces. In fact, because the length of the L-shaped wing is small and there is little conflict with concrete, these models are not very effective. But it can be seen that when the length of the L-shaped is large, the efficiency of the model is greatly improved. Again, it can be seen that the performance of models with T-shaped studs is better than models with L-shaped studs.

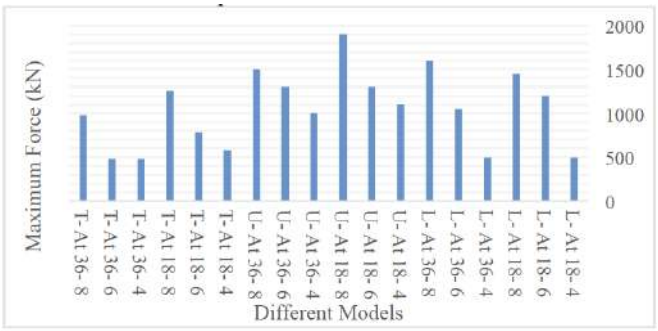

Figure 41: Comparison of maximum tolerable forces in different models.

In Table **5**, a comparison between the percentages of force increases and tolerable displacements of different models is presented. These percentages have been compared to the resistance of the CFT column model without a stud, which is presented in Figure **36**. As can be seen, when the length of the stud is short (in this study, 4 cm), there is no increase in the amount of tolerable displacement, and the forces also increased slightly. The biggest increases are related to models with the U-shaped stud, for which the forces have increased by 295%, and then models with the L-shaped stud, in which the forces have increased by 233%. The largest increase in displacement also belongs to U-shaped studs, which showed a 31.58% increase.

4. CONCLUSION

After analyzing the models and comparing the obtained outputs, the following results are obtained. In terms of strain energy and plastic energy, although the

Table 5: Comparison of Different Model Responses with Changing stud Properties Versus the Model without a Shear Stud

Model name	Maximum displacement	Maximum Force	Displacement increase %	Resistance increase %
L- At 18- 4	0.038	500	0.00%	4.17%
L- At 18- 6	0.039	1200	2.63%	150%
L- At 18- 8	0.038	1450	0.00%	202%
L- At 36- 4	0.038	500	0.00%	4.17%
L- At 36- 6	0.04	1050	5.26%	118.75%
L- At 36- 8	0.04	1600	5.26%	233.33%
U- At 18- 4	0.038	1100	0.00%	129.17%
U- At 18- 6	0.04	1300	5.26%	170.83%
U- At 18- 8	0.05	1900	31.58%	295%
U- At 36- 4	0.04	1000	5.26%	108%
U- At 36- 6	0.04	1300	5.26%	170%
U- At 36- 8	0.05	1500	31.58%	212%
T- At 18- 4	0.04	580	5.26%	20.83%
T- At 18- 6	0.04	780	5.26%	62.5%
T- At 18- 8	0.04	1250	5.26%	160%
T- At 36- 4	0.038	480	2.63%	0.00%
T- At 36- 6	0.04	480	5.26%	0.00%
T- At 36- 8	0.038	980	0.00%	104%

energy value of models with a T-shaped stud is higher, it is in a range close to other models, and the values of these two energies are almost the same for all models. The internal energy of T-At18-8 and T-At18-6 models is more than all other models. After that, U-At18-8 and T-At18-6 models have the highest internal energy values. Also, models with L-shaped studs have the lowest amount of internal energy compared to other models, and models that have any shape of studs with a size of 4 cm also have a small amount of energy. The curves related to the force-displacement diagram of models with U-shaped studs and with 36 cm intervals along the column have a lot of irregularity, and indiscretion is much more noticeable in these models. Models with T-shaped studs and 18 cm intervals along the column height, unlike other models, have shown almost the same performance in tensile and compressive cycles in terms of ultimate force. The main reason for this is the greater continuity of the stud compared to other kinds of studs. Force-displacement curves of T-At 36-6 and T-At 36-8 models show very favorable behavior, due to an increase in the area inside the cycles. The amount of force that can be tolerated by the models with the T-shaped stud is higher than other models. Also, unlike models with the L-shaped studs that performed poorly in tensile cycles, these models are very strong in tensile cycles, and the reason for this is the proper connection of concrete and stud due to the geometry of T-shaped studs. When the length of the stud is extended to 8 cm and the distance between the studs in the longitudinal axis of the column increases, although the tolerable force values increase in the tensile area of the diagram, but when the direction of applied load is changed, in compression cycles that creates the pressure in the models, the tolerable force values are greatly reduced. Models in which the distance of studs is 36 cm from each other, at the beginning, have almost the same load as the models with studs of the same size and distance of 18 cm in the longitudinal axis of the column, but in the compression cycles, the values of the tolerable forces are greatly reduced. In all models with 4 cm height studs, the force-displacement curves have many irregularities and do not have regular cycles. With the increase in the length of the studs, the cycles have become more regular, and the force-displacement values have also increased.

REFERENCES

Amer, M., Chen, Z., Du, Y., Mashrah, W. A. H., & Zhang, W. (2023). Experimental and numerical investigations on cyclic performance of L-shaped-CFT column frame-buckling restrained and unrestrained steel plate shear walls with partial double-side/four corner connections. *Journal of Building Engineering*, *78*, 107568. https://doi.org/10.1016/j.jobe.2023.107568

Borzoo, S., Ghaderi, S. R. M., Mohebi, S., & Rahimzadeh, A. (2016). Nonlinear finite element modeling of steel-sheathed cold-formed steel shears walls. *Steel Compos. Struct*, *22*(1), 79–89. https://doi.org/10.12989/scs.2016.22.1.079

Ding, F.-X., Fu, L., Liu, X.-M., & Liu, J. (2016). Mechanical performances of track-shaped rebar stiffened concrete-filled steel tubular (SCFRT) stub columns under axial compression. *Thin-Walled Structures*, *99*, 168–181. https://doi.org/10.1016/j.tws.2015.11.022

Guo, X., Zhang, C., Luo, J., Zhang, Y., Chen, S., & Gao, S. (2023). Experimental and numerical investigations on large-section rectangular CFT columns with distributive beam under axial compression. *The Structural Design of Tall and Special Buildings*, *32*(2), e1989. https://doi.org/10.1002/tal.1989

Habibi, A., Fanaie, N., & Shahbazpanahi, S. (2023). Experimental and numerical investigation of I-beam to concrete-filled tube (CFT) column moment connections with pipe-stiffened internal diaphragm. *Journal of Constructional Steel Research*, *200*, 107648. https://doi.org/10.1016/j.jcsr.2022.107648

Huang, W.-F., Shao, Y.-B., & Hassanein, M. F. (2023). Behaviour and confinement-based direct design of concrete-filled cold-formed stiffened steel tubular short columns. *Journal of Constructional Steel Research*, *202*, 107773. https://doi.org/10.1016/j.jcsr.2022.107773

Li, J., Mou, B., & Wang, Z. (2023). Cyclic behavior of column-to-column connections in novel prefabricated H-shaped steel beam to CFST column joint. *Journal of Constructional Steel Research*, *200*, 107657. https://doi.org/10.1016/j.jcsr.2022.107657

Lin, Y., Ye, Q., Wang, Y., Shu, C., Zhang, F., Zhang, Y., Zhao, Y., & Cao, H. (2023). Seismic behaviour of diaphragm-through bolted-welded joints between CFST column to steel beam. *Journal of Constructional Steel Research*, *200*, 107651. https://doi.org/10.1016/j.jcsr.2022.107651

Najafi, S., & Borzoo, S. (2022). Different strengthening designs and material properties on bending behavior of externally reinforced concrete slab. *Structural Monitoring and Maintenance*, *9*(3), 271–287.

Najafi, S., Borzoo, S., Saboohian, K., & Aboutalebi, H. (2025). Evaluation of seismic performance of steel frames with Y-shape braces under far-field and near-field earthquakes. *Numerical Methods in Civil Engineering*, *9*(4), 41–50. https://doi.org/10.61186/NMCE.2505.1088

Najafi, S., Saboohian, K., & Borzoo, S. (2022). The Effect of Y-Shaped Brace Configuration on Its Seismic Behavior. *International Journal of Steel Structures*, 1–19. https://doi.org/10.1007/s13296-021-00566-y

Nguyen-The, D., Thai, S., Nguyen-Van, H., & Ngo-Huu, C. (2024). Numerical Modelling of the Punching Shear Response of Shearhead Connections between a CFT Column and a Flat Reinforced Concrete Slab. *Structural Engineering International*, 1–15. https://doi.org/10.1080/10168664.2024.2416474

Pahlavannejad Tabarestani, N., Naghipour, M., & Hicks, S. J. (2025). Compressive Behavior of Long Simple and Multi-Cell CFT Columns When Using Tie Bars Connector Elements. *Buildings*, *15*(5), 817. https://doi.org/10.3390/buildings15050817

Razavi, S. A., Kandi, A. H., Alimardani, M., & Jovaini, E. (2023). Tube-in-tube rigid beam to CFT column connection in moment-resisting frames: An experimental study. *Soil Dynamics and Earthquake Engineering*, *171*, 107901. https://doi.org/10.1016/j.soildyn.2023.107901

Song, S., Son, D.-H., Bae, B.-I., Um, S.-S., & Choi, C.-S. (2024). Axial load behavior of CFT columns assembled with rectangular wave-shaped ribs. *Structures*, *61*, 106027. https://doi.org/10.1016/j.istruc.2024.107324

Wang, B., Liang, J., & Lu, Z. (2019). Experimental investigation on seismic behavior of square CFT columns with different shear stud layout. *Journal of Constructional Steel Research*, *153*, 130–138. https://doi.org/10.1016/j.jcsr.2018.10.004

Zhou, Z., Denavit, M. D., & Zhou, X. (2023). New cross-sectional slenderness limits for stiffened rectangular concrete-filled steel tubes. *Engineering Structures*, *280*, 115689. https://doi.org/10.1016/j.engstruct.2023.115689

Received on 17-09-2025 Accepted on 04-11-2025 Published on 12-11-2025

https://doi.org/10.65904/3083-3604.2025.01.04